Inorganic Chemistry

Article

pubs.acs.org/IC

Hydroxide Ion versus Chloride and Methoxide as an Exogenous Ligand Reveals the Influence of Hydrogen Bonding with Second-Sphere Coordination Water Molecules in the Electron Transfer Kinetics of Mn Complexes

Sanae El Ghachtouli,[†,‡] Régis Guillot,[‡] Ally Aukauloo,[‡,▽] Pierre Dorlet,[▽,§] Elodie Anxolabéhère-Mallart,*[,†] and Cyrille Costentin[†]

[†]Laboratoire d'Electrochimie Moléculaire, Univ Paris Diderot, Sorbonne Paris Cité, Unité Mixte de Recherche Université−CNRS No. 7591, Bâtiment Lavoisier, 15 rue Jean de Baïf, 75205 Paris Cedex 13, France

[‡]ICMMO−UMR 8182−Bât. 420, Université Paris−Sud 11, 15 rue Georges Clemenceau, 91405 Orsay Cedex, France

[§]Laboratoire Stress Oxydant et Détoxication, CNRS, UMR 8221, F-91191 Gif-sur-Yvette, France

[▽]CEA, iBiTec-S, SB²SM, F-91191 Gif-sur-Yvette, France

Supporting Information

ABSTRACT: We recently reported on the synthesis of a new pentadentate N_4O ligand, *tBu*L$^-$, together with the X-ray diffraction structure of the corresponding mononuclear manganese(III)-hydroxo complex namely [(*tBu*L)Mn(III)OH]-(ClO_4), (**1** (ClO_4)). [El Ghachtouli et al. *Energy Environ. Sci.* **2011**, *4*, 2041.] In the present work, we evidence through electrochemical analysis that complex **1**$^+$, in the presence of water, shows a peculiar behavior toward electron-transfer kinetics. The synthesis, single-crystal X-ray diffraction, and EPR spectroscopic characterization of two other mononuclear manganese(III)-chlorido and methoxo complexes—namely, [(*tBu*L)Mn(III)Cl](PF_6), (**2**(PF_6)) and [(*tBu*L)Mn(III)OMe](ClO_4), (**3**(ClO_4))—are also reported. **2**(PF_6) and **3**(ClO_4) compounds will serve as reference complexes for the electron-transfer kinetics investigation. The peculiar behavior of **1**(ClO_4) is attributed to the specificity of hydroxide anion as ligand presumably allowing intermolecular hydrogen-bonding interactions and thus affecting electron-transfer properties.

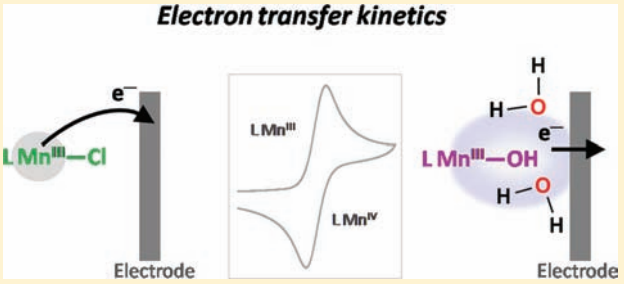

INTRODUCTION

Manganese complexes have long been used as models for one of the most intricate metalloenzyme's active site, the Oxygen Evolving Complex (OEC) of Photosystem II.[2] This Mn_4Ca complex performs the four-electron, four-proton oxidation of water, following a five-step catalytic cycle called the Kok cycle. Although the structure of the OEC in its resting state currently is fairly well-understood,[3−7] questions remain as to the mechanism by which two water molecules are oxidized into dioxygen at this cluster.[8−13] This catalysis is thought to involve formation of a high-valency manganese oxo species.[12,14] In the endeavor to identify the ultimate species prior the formation of the O−O bond, mononuclear manganese model complexes play a critical role.[15] They provide basic information on the relationship between manganese and water, when oxidation events occur. Along this line, several groups[16−19] have designed different families of ligands that accommodate the manganese ion in a high-valency, mononuclear state, while a water molecule (in its protonated or deprotonated form) is bound to it.

We recently reported on the synthesis of a new pentadentate N_4O ligand, *tBu*L$^-$ (Scheme 1), together with the X-ray diffraction (XRD) structure of the corresponding mononuclear manganese(III)-hydroxo complex namely [(*tBu*L)Mn(III)-OH](ClO_4), (**1** (ClO_4)).[1] Electrochemical studies of **1**$^+$ clearly evidenced that the presence of outer sphere water molecules is essential for the reversibility of the $Mn^{III/II}$ and $Mn^{IV/III}$ redox processes, thus inhibiting deleterious pathways. In particular, in this last case, the electron transfer is not accompanied by

Scheme 1. Schematic Representation of LH and *tBu*LH

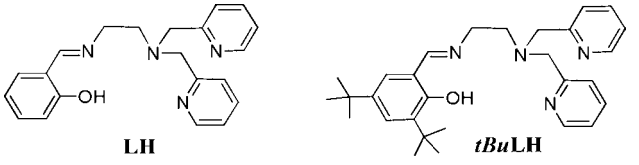

Received: November 17, 2011
Published: March 8, 2012

   dx.doi.org/10.1021/ic202480h | *Inorg. Chem.* 2012, 51, 3603−3612

proton transfer. In the present study, we investigate the electron transfer dynamics of these redox processes with the aim to get new insights into the role of the hydroxo ligand, and, in particular, the possible influence of intermolecular bonding interactions. We have thus prepared two new mononuclear manganese(III)-chlorido and manganese(III)-methoxo complexes, namely, [(*tBu*L)Mn(III)Cl](PF$_6$), **2**(PF$_6$) and [(*tBu*L)-Mn(III)OMe](ClO$_4$), **3**(ClO$_4$), which are identical to **1**(ClO$_4$), except for the sixth ligand. We first report on the solid-state structural characterization of both chloro and methoxo Mn(III) complexes and compare them with the previously reported hydroxo compound. Parallel-mode EPR studies indicate that a mononuclear form is maintained in MeCN solution for all Mn(III) complexes. Electrochemical investigation is then used to access the +IV oxidation state for **2**$^+$ and **3**$^+$ and the +II and +IV oxidation states for **1**$^+$. All Mn(IV) compounds are shown to be mononuclear species, using electronic absorption and EPR spectroscopies. The latter also allows one to gain insights into structure and electronic properties homogeneity in solution for the complexes studied. Finally, thanks to the cyclic voltammetry measurements performed at various temperatures, the electron transfer dynamics parameters for all three complexes are obtained. It will be shown that complex **1**$^+$ has, in the presence of water, a peculiar behavior toward electron transfer kinetics attributed to the specificity of hydroxide anion as ligand, presumably allowing intermolecular hydrogen bonding interactions, thus affecting electron transfer properties.

EXPERIMENTAL SECTION

Caution: Perchlorate salts of metal complexes with organic ligands are potentially explosive. Only small quantities of these compounds should be prepared, and they should be handled behind suitable protective shields.

Reagents and solvents were purchased commercially and used as received.

Ligand Synthesis. *tBuLH.* To a solution of 451 mg (1.86 mmol) of *N,N-bis*(2-pyridylmethyl)ethane-1,2-diamine[20] in 50 mL of ethanol was added 1 equiv of 3,5-di-*tert*-butyl-2-hydroxybenzaldehyde.[21] The solution was stirred at room temperature for 3 h. The solvents were evaporated and the resulting brown oil was dried under vacuum. The crude product was purified by flash chromatography (CH_2Cl_2/MeOH) to yield the ligand *tBu*LH as a yellow solid (75% yield): ^{1}H NMR (300 MHz, $CDCl_3$): δ 11.66 (s, 1H, OH), 8.52 (d, 2H, H−Ar), 8.29 (s, 1H, Ar−CH═N), 7.61−7.04 (m, 8H, H−Ar), 3.94 (s, 4H, N−(CH_2−Py)2), 3.75 (t, 2H, CH═N−CH_2−CH_2), 2.95 (t, 2H, (CH_2)$_2$−N−CH_2−CH_2), 1.49 (s, 9H, H−*tBu*), 1.34 (s, 9H, H−*tBu*).

Synthesis of Complexes. *[tBuLMn(III)OH](ClO$_4$) (**1**(ClO$_4$)).* [*tBu*LMn(III)OH](ClO$_4$)] (**1**(ClO$_4$)) was prepared according to the recently published procedure.[1]

*[tBuLMn(III)Cl](PF$_6$)] (**2** (PF$_6$)).* To a solution of ligand *tBu*LH (73 mg, 0.16 mmol) in methanol (5 mL) and triethylamine (22.15 μL, 0.16 mmol) were added 31.5 mg of Mn(Cl)$_2$·4(H$_2$O) (0.16 mmol) in methanol (2 mL).The mixture was stirred for 3 h at room temperature. Two equivalents (2 equiv) of NH_4PF_6 (51.96 mg, 0.32 mmol) were then added onto the brown solution, which was stirred for an additional 3 h. The mixture was then filtered and the resulting solution was kept at room temperature. After one week, brown crystals deposited from this solution (yield 60%). Elemental analysis for [Mn(tBuL)Cl](PF$_6$): $MnC_{29}H_{37}N_4PF_6O$ Calcd (%): C 50.26, H 5.38, N 8.08; Found (%): C 50.02, H 5.40, N 8.21. ESI MS: m/z = 547 [(*tBu*L)MnCl]$^+$. IR (KBr): ν = 1542 (weak,w), 1449 (w), 1252 (w), 1020 (w), 845 (strong, s), 557 cm^{-1} (PF$_6^-$).

*[tBuLMn(III)OMe](ClO$_4$) (**3**(ClO$_4$)).* To a solution of ligand *tBu*LH (73 mg, 0.16 mmol) in methanol (5 mL), 1 equiv of triethylamine (22.15 μL, 0.16 mmol) was added, followed by 1 equiv of Mn(ClO$_4$)$_2$·6(H$_2$O) (55.8 mg, 0.16 mmol) in methanol (2 mL). The mixture was stirred for 3 h at room temperature. Twenty milliliters (20 mL) of diethylether were added to the solution, leading to the formation of a green precipitate. The suspension was filtered off and the solid was washed with diethylether and minimal cold methanol. The resulting powder was dissolved in methanol and slow diffusion of diethylether yielded green needles (overall yield 65%). Elemental analysis for [*tBu*LMn(III)OMe](ClO$_4$)]: $MnC_{30}H_{40}N_4ClO_6$ Calcd (%): C 56.03, H 6.27, N 8.71; Found (%): C 55.53, H 6.25, N 8.73. ESI MS: m/z = 543.3 [(*tBu*L)Mn(III)-OCH$_3$]$^+$. IR (KBr): ν = 1542 (weak, w), 1449 (w), 1252 (w), 1120, 1085 (s), 1020 (w), 640 (ClO$_4^-$), 609 (w).

Elemental Analyses. Elemental analyses were carried out at the Service de Microanalyses, ICSN-CNRS, Gif-sur-Yvette, France.

Electrospray Ionization Mass Spectrometry. Mass spectra were recorded with a Finnigan MAT95S system in a BE configuration at low resolution on a micromolar acetonitrile solution.

NMR Spectroscopy. ^{1}H NMR spectra were recorded on a Bruker DPX 300 MHz system with a ONP probe at room temperature in d_1-$CDCl_3$ (δ = 7.24 ppm).

EPR Spectroscopy. 9.4 GHz EPR (X-band) spectra were recorded on a Bruker ELEXSYS 500 spectrometer equipped with an Oxford Instruments continuous-flow liquid-helium cryostat and a temperature control system. A dual-mode cavity (Bruker, Model ER 4116DM) was used for perpendicular- and parallel-mode detection, respectively. Solutions spectra were recorded in MeCN containing 0.2 M Bu_4NPF_6. Simulations were performed using Easyspin[22] or the Xsophe software (v4.0).[23]

Ultraviolet−Visible (UV−Vis) Light Analysis. Ultraviolet−visible (UV−Vis) spectra were recorded on a Varian Cary 300 Bio spectrophotometer at 20 °C with 0.1 cm quartz cuvettes.

Spectroelectrochemistry. Spectroelectrochemical data were obtained using a combination of a three-electrode thin cell (optical length = 0.5 mm) mounted in an ultraviolet/visible light/near infrared (UV/Vis/NIR) Varian Cary 5E spectrophotometer. The two-part spectroelectrochemical 0.5-mm quartz cell has been described elsewhere.[24] The working electrode is a Pt grid, and the reference and the counter electrodes (Pt wire) are located on the top of the cell. The entire solution was under an argon environment.

Cyclic Voltammetry and Bulk Electrolysis. All electrochemical experiments were operated under an argon atmosphere. Cyclic voltammetry and coulometry measurements were recorded either on an EGG PAR potentiostat (M273 model) or a Metrohm potentiostat (AUTOLAB model). For cyclic voltammetry, the counter electrode used was a Pt wire and the working electrode a glassy carbon disk carefully polished before each voltammogram with a 1-μm diamond paste, sonicated in ethanol bath and then washed with ethanol. The reference electrode used was an Ag/AgClO$_4$ electrode (0.3 V vs SCE electrode), isolated from the rest of the solution by a fritted bridge. The ohmic drop was systematically compensated using the adequate option within the commercial potentiostat. The effect of ohmic drop compensation on peak potentials was tested on a ferrocene solution, as described in the Supporting Information. For bulk electrolysis, the counter electrode used was a piece of platinum, separated from the rest of the solution with a fritted bridge. The working electrode was a cylinder of glassy carbon. The supporting electrolyte NBu_4PF_6 (Aldrich, puriss) was 0.1 M (20 °C) or 0.2 M (low temperature) in acetonitrile (Aldrich, puriss). Low-temperature regulation was ensured by a Julabo circulation cryostat.

X-ray Diffraction. X-ray diffraction (XRD) data were collected on a Kappa X8 APPEX II Bruker diffractometer with graphite-monochromated Mo Kα radiation (λ = 0.71073 Å). The temperature of the crystal was maintained at the selected value (100 K) by means of a 700 series Cryostream cooling device within an accuracy of ±1 K. The data were corrected for Lorentz polarization and absorption effects. The structures were solved by direct methods using SHELXS-97[25] and refined against F^2 by full-matrix least-squares techniques

dx.doi.org/10.1021/ic202480h | Inorg. Chem. 2012, 51, 3603−3612

using SHELXL-97 with anisotropic displacement parameters for all non-hydrogen atoms. H atoms of the ligand were added geometrically and refined by the riding model. Treatment on H: H atoms of water moieties were added from the difference Fourier map, and refined by DFIX instructions, in which O−H distances were set at 0.96(3) Å and H−H distances were set at 1.52(3) Å, according to the ideal molecular geometry of water, and with one common isotropic thermal parameter. All calculations were performed by using the Crystal Structure crystallographic software package WINGX.[26] ORTEP view of 2^+ and 3^+ are shown in Figure S1 in the Supporting Information and selected bond lengths and angles for 1^+, 2^+, and 3^+ can be found in Table S1 in the Supporting Information. Crystallographic data for 2^+ and 3^+ are gathered in Table S2 in the Supporting Information.

CCDC 781530 and CCDC 781529 contains the supplementary crystallographic data for $2(PF_6)$ and $3(ClO_4)$. These data can be obtained free of charge from The Cambridge Crystallographic Data Centre viawww.ccdc.cam.ac.uk/data_request/cif.

RESULTS AND DISCUSSION

Synthesis. The mononuclear Mn(III) complex [*tBu*LMn(III)OH](ClO_4)(**1** (ClO_4)) was prepared following a template synthesis in ethanol, with Mn(II) perchlorate as the source of manganese. [*tBu*LMn(III)Cl](PF_6) (**2** (PF_6)) was obtained by reacting *tBu*LH with manganese(II) chloride in acetonitrile in the presence of 1 equiv of base and isolated in the presence of hexafluorophosphate. [*tBu*LMn(III)OMe](ClO_4)] (**3** (ClO_4)) was obtained under similar conditions in methanol. Brown, red, and green single crystals were grown for **1**(ClO_4), **2**(PF_6), and **3**(ClO_4), respectively (see the Experimental Section).

X-ray Diffraction. Although they have been reported in a recent paper,[1] in this paper, we include the crystallographic data for **1**(ClO_4), in order to facilitate comparison with **2**(PF_6) and **3** (ClO_4). The crystal structures of **2**(PF_6) and **3**(ClO_4) were determined by single-crystal X-ray diffraction (Figure 1). Table 1 gather selected bond lengths for 1^+, 2^+, and 3^+. In all three complexes, the Mn^{3+} ion is hexacoordinated by the N_4O ligand and by the exogenous ligand. The two pyridine arms are in the *trans* positions. The Jahn−Teller axis is elongated along the $N_{pyridine}$−Mn−$N_{pyridine}$ axis, which forms an angle of 152° in all three complexes (see Table S1 in the Supporting Information). This type of coordination has always prevailed in related systems,[18] such as that for the parent ligand L^- (see Scheme 1).[20,27,28] In all three complexes, the Mn−N_{imine} (d = 1.97−1.99 Å) and the Mn−$O_{phenolate}$ (d = 1.85−1.89 Å) distances are comparable to those reported for Mn(III) complexes in a similar environment.[20,29−31]

In the case of 1^+, two distinct mononuclear units are present in the cell, featuring two different Mn−$O_{hydroxide}$ bonds (1.97(3) Å and 1.86(3) Å), because of a hydrogen bond with interstitial water molecules.[1] Both distances are larger than most of the reported manganese(III)-hydroxo complexes (1.80− 1.81 Å).[17,18,32−34] The structure of 2^+ is very similar to that of $[LMn(III)Cl]^+$,[27] except for the Mn−Cl bond (mean value 2.25 Å, vs 2.265 Å), which is 0.01 Å shorter. This shortening is opposite to what would be expected from the electron-donating effect of the *tert*-butyl groups. However, we noticed the arrangement in the crystal lattice of two monomeric units face-to-face, with two pyridine rings stacked upon each other at a distance of 3.91 Å and the chloride ligand interacting with a hydrogen atom (at 2.74 Å) of the latter pyridine ring. These weak intermolecular interactions may account for the unexpected shortening of the Mn−Cl bond, compared to the unsubstituted ligand L^-. Without any noticeable intermolecular interactions, complex 3^+ presents a mean Mn−$O_{methoxide}$ bond

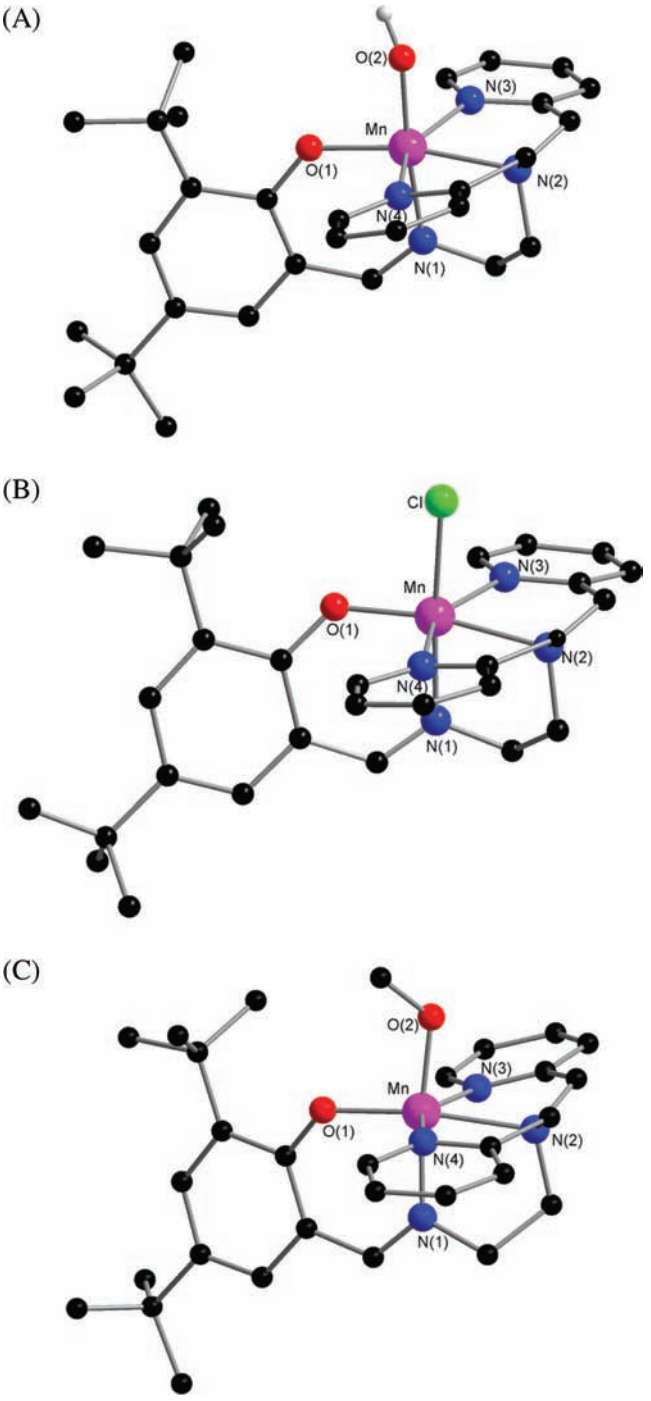

Figure 1. X-ray crystal structure of cations (A) 1^+, (B) 2^+, and (C) 3^+. Hydrogen atoms (except for the hydroxide ligand), counteranions, and solvent molecules were omitted for the sake of clarity.

of 1.81 Å, which is close to the Mn(III)−OH bond distances reported so far, but shorter than the Mn−$O_{hydroxide}$ bonds in both isomers of 1^+. This, again, points at the peculiar structure of 1^+, in which the elongation of the Mn−O bond is clearly related to intermolecular hydrogen bonding interactions. The main difference between these three complexes lies in the Mn−X (X = OH^-, Cl^-, MeO^-) distance, which is either modulated by the electron-donating abilities of the exogenous ligand (long Mn−X bond for weaker ligands such as Cl^-) or by intermolecular interactions (hydrogen bonds between hydroxide ligand and water molecules in the case of 1^+).

dx.doi.org/10.1021/ic202480h | Inorg. Chem. 2012, 51, 3603−3612

Table 1. Selected Bond Lengths for 2^+ and 3^+ (Data for Complex 1^+ have been included, for the sake of comparison) (ref 1)

bond	bond length (Å)	bond	bond length (Å)
	1^+ = [Mn(tBuL)OH]$^{+a}$		
Mn−O(1)	1.88(3)	Mn−N(3)	2.23(4)
Mn−N(1)	1.97(4)	Mn−N(4)	2.22(4)
Mn−N(2)	2.16(4)	Mn−O(2)	1.91(3)
	2^+ = [Mn(tBuL)Cl]$^+$		
Mn−O(1)	1.859(2)	Mn−N(3)	2.252(3)
Mn−N(1)	1.990(3)	Mn−N(4)	2.250(3)
Mn−N(2)	2.148(3)	Mn−Cl	2.2568(9)
	3^+ = [Mn(tBuL)OMe]$^+$		
Mn−O(1)	1.895(6)	Mn−N(3)	2.264(9)
Mn−N(1)	1.988(8)	Mn−N(4)	2.237(9)
Mn−N(2)	2.150(8)	Mn−O(2)	1.814(7)

^{a}Two structural motifs were found in the unit cell; thus, the given distances are mean values between site 1 and site 2 of the unit.

Electrochemical Characterization and Access to Mn(IV) Complexes. Cyclic voltammetry of $1(ClO_4)$ (Figure 2A), $2(PF_6)$ (Figure 2B), and $3(ClO_4)$ (Figure 2C) were recorded in acetonitrile. The trace of cation 1^+ presents a quasi-reversible anodic process at $E^0(1)$ = 0.80 V vs SCE (ΔE_p = 200 mV at 0.1 V s^{-1}), attributed to the Mn(III) to Mn(IV) oxidation process and an irreversible cathodic process (see Figure S2(A) in the Supporting Information) at $E_p(1)$ = −0.52 V vs SCE). As reported earlier,[1] in dry acetonitrile, this oxidation wave is not chemically reversible: full reversibility is obtained upon the addition of water. The trace of cation 2^+ also shows a quasi-reversible oxidation process attributed to the Mn(III) to Mn(IV) at $E^0(2)$ = 1.10 V vs SCE (ΔE_p = 96 mV at 0.1 V s^{-1}) (see Table 2) and a quasi-reversible cathodic process at $E^0(2')$

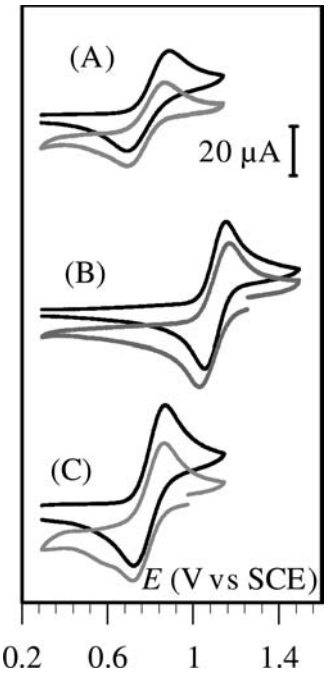

Figure 2. Cyclic voltammetry for a 2 mM solution in CH_3CN (0.1 M Bu_4NPF_6) of (A) $1(ClO_4)$ + 15.8 M of water, before (black line) and after (gray line) exhaustive oxidative electrolysis at +1.00 V vs SCE; (B) **2** (PF_6) before (black line) and after (gray line) exhaustive oxidative electrolysis at +1.25 V vs SCE; and (C) **3** (ClO_4), before (black line) and after (gray line) exhaustive oxidative electrolysis at +0.975 V vs SCE. Scan rate = 100 mV s^{-1}, T = 293 K.[1,36]

Table 2. E^0 (or E_p) Values^a (V vs SCE) for Cations 1^+, 2^+, and 3^+ in CH_3CN (0.1 M Bu_4NPF_6) and Related Complexes

	Mn^{III}/Mn^{II}		Mn^{IV}/Mn^{III}	
	E^0 or E_p	ΔE_p (mV)	E^0	ΔE_p (mV)
1^+	−0.52	irr	0.80	200
2^+	0.10	100	1.10	96
3^+	−0.58	irr	0.80	235
$1H^{2+}$	0.30	300		

$^aE^0$ is defined as $(E_p^a + E_p^c)/2$, where E_p^a is the potential value of the anodic peak and E_p^c is the potential value of the cathodic peak.

= 0.10 V vs SCE (ΔE_p = 100 mV at 0.1 V s^{-1}), attributed to the Mn(III) to Mn(II) reduction process (Figure S2(B) in the Supporting Information). The trace of complex 3^+ (anodic process at $E^0(3)$ = 0.80 V vs SCE and irreversible cathodic process at $E_p(1)$ = −0.58 V vs SCE; see Figure S2(C) in the Supporting Information) is similar to that of complex 1^+, except for a slightly slower electron transfer, as indicated by a larger ΔE_p value (235 mV at 0.1 V s^{-1}). The observation of three distinguishable signatures for complexes 1^+, 2^+, and 3^+ supports the assertion that the exogenous ligand is maintained in the coordination sphere in acetonitrile solution.[35] In addition, cations 1^+, 2^+, and 3^+ were detected by EI-MS spectrometry (see the Experimental Section). Standard potential (or peak potential for chemically irreversible couples) values for complexes 1^+, 2^+, and 3^+ are gathered in Table 2. No difference in potential is observed between the hydroxo complex 1^+ and the methoxo complex 3^+. Thus, the noticeably higher potential value observed for 2^+ can be attributed to a weaker donating effect of the Cl^- anion to the Mn^{3+} cation, compared to hydroxo and methoxo ligands, corroborating the Mn−X (X = OH^-, Cl^-, MeO^-) distances observed in the X-ray structures.

We have demonstrated that, provided water is present in the medium to prevent dimerization, complex 1^+ undergoes a simple outersphere electron transfer upon oxidation.[1] The addition of a strong acid ($HClO_4$) to a solution containing the hydroxo complex 1^+ in an acetonitrile−water mixture leads to a decrease and complete disappearance of the wave (Figure 3, peaks 1 and 1′) at the expense of a new one (Figure 3, peaks 2 and 2′). This is attributed to the protonation of the hydroxo ligand in complex 1^+, leading to a shift of the oxidation potential toward a more-positive potential. Indeed, an irreversible wave is detected at ∼1.1 V vs SCE, which is attributed to the oxidation process of the protonated form $[Mn(III)(OH_2)]^{2+}$ (see Figures S3 and S4 in the Supporting Information). Conversely, reduction of $[Mn(III)(OH_2)]^{2+}$, hereafter named $1H^{2+}$, becomes easy and leads to a monoelectronic chemically reversible $[Mn(III)(OH_2)]^{2+}$/ $[Mn(II)(OH_2)]^+$ wave, whose characteristics are given in Table 2.

We performed exhaustive bulk electrolysis of $1(ClO_4)$, $2(PF_6)$, and $3(ClO_4)$, in acetonitrile at 20 °C, at +1.00, +1.25, and +0.975 V vs SCE, respectively. In each case, controlled potential coulometric measurements confirmed a one-electron oxidation process. The cyclic voltammograms recorded on the electrolyzed solutions of $1(ClO_4)$, $2(PF_6)$, and $3(ClO_4)$ show traces (gray lines in Figure 2) that are identical to those of the initial solutions. This indicates a simple electron transfer and identifies the oxidation products as [*t*BuLMn(IV)-

dx.doi.org/10.1021/ic202480h | Inorg. Chem. 2012, 51, 3603−3612

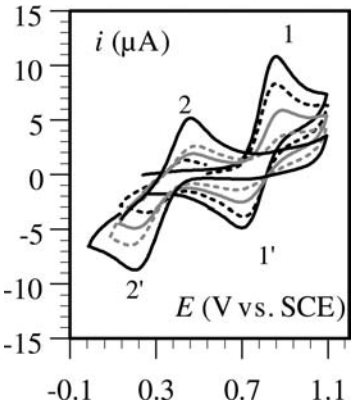

Figure 3. Cyclic voltammetry of $\mathbf{1}^{+}$ (1 mM) at 0.1 V s^{-1}, T = 293 K, on a glassy carbon electrode (GCE) in a CH_3CN/H_2O mixture (75/25 v/v) + 0.1 M NBu_4PF_6 (wave 1/1′, black curve) and in the presence of an increasing amount of $HClO_4$ (0.25 equiv (black dashed curve), 0.5 equiv (gray curve), 0.75 equiv (gray dashed curve), and 1 equiv (wave 2/2′, black curve)).

$(OH)]^{2+}$ (hereafter named $\mathbf{1}^{2+}$), $[t\mathit{Bu}LMn(IV)(Cl)]^{2+}$ (hereafter named $\mathbf{2}^{2+}$), and $[t\mathit{Bu}LMn(IV)(OMe)]^{2+}$ (hereafter named $\mathbf{3}^{2+}$), respectively. In all cases, the one-electron oxidation process is associated with a color change from brown (for $\mathbf{1}^{+}$ and $\mathbf{3}^{+}$) and reddish (for $\mathbf{2}^{+}$) to intense dark green. The oxidized species are stable for several hours under these conditions. In the following paragraphs, we will present solution characterization of these three electrochemically generated complexes $\mathbf{1}^{2+}$, $\mathbf{2}^{2+}$, and $\mathbf{3}^{2+}$, using parallel- and perpendicular-mode electron paramagnetic resonance (EPR) and electronic absorption spectroscopies.

EPR Spectroscopy. X-band EPR spectra have been recorded for complexes $\mathbf{1}^{+}$, $\mathbf{2}^{+}$, and $\mathbf{3}^{+}$ in acetonitrile solution, as well as for the corresponding complexes $\mathbf{1}^{2+}$, $\mathbf{2}^{2+}$, and $\mathbf{3}^{2+}$ obtained after bulk electrolysis, as described in the previous section. The spectra obtained are shown in Figures 4 (complexes $\mathbf{1}^{+}$ and $\mathbf{3}^{+}$) and 5 (complex $\mathbf{2}^{+}$). Before electrolysis, the spectra for $\mathbf{1}^{+}$, $\mathbf{2}^{+}$, and $\mathbf{3}^{+}$ display predominantly a signal in parallel-mode detection (right panel) consistent with a Mn(III) mononuclear complex (a six-line hyperfine splitting of ~5 mT can be resolved on all three spectra for the feature centered at 81 mT; see the right panel in Figures 4 and 5 and Figure S5 in the Supporting Information).[37] The corresponding perpendicular-mode spectra are essentially silent for $\mathbf{1}^{+}$ and $\mathbf{3}^{+}$ (see Figure 4, left panel). In the case of $\mathbf{2}^{+}$(Figure 5, left panel), we note the presence of some "free" Mn(II) (characteristic six-line signal at g = 2; the amount was estimated by titration to be <10% of the total Mn content) and of a signal at low field (0−150 mT) attributable to "forbidden" transitions from the Mn(III) complex. The parallel-mode signals of the Mn(III) complexes essentially disappear upon electrolysis ($\mathbf{1}^{2+}$, $\mathbf{3}^{2+}$ in the right panel of Figure 4, $\mathbf{2}^{2+}$ in the right panel of Figure 5), while new signals characteristic of an $S = {}^{3}/_{2}$ mononuclear Mn(IV) complex are now detected in perpendicular mode (respective left panels). We also note the disappearance of the low field signal from the perpendicular-mode spectrum of $\mathbf{2}^{+}$ (Figure 5, left panel), supporting its attribution to Mn(III) resonances. In the case of $\mathbf{2}^{2+}$, the feature around 130 mT displays a well-resolved six-line hyperfine splitting of 6.4 mT consistent with a manganese ion in the tetravalent oxidation state (+IV), similar to that which has been reported for a $[(salen)Mn(IV)Cl]^{+}$ complex (see Figure 5, upper left panel).[38] In the case of $\mathbf{1}^{2+}$

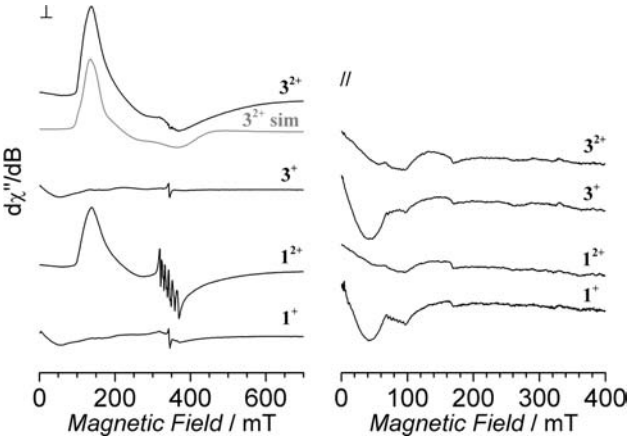

Figure 4. EPR spectra recorded for the hydroxo and methoxo complexes with perpendicular-mode (left) and parallel-mode (right) detection before (complexes $\mathbf{1}^{+}$ and $\mathbf{3}^{+}$) and after (complexes $\mathbf{1}^{2+}$ and $\mathbf{3}^{2+}$) exhaustive electrolysis at +0.99 and +0.975 V vs SCE, respectively. Experimental conditions: 2 mM solution in CH_3CN (0.1 M Bu_4NPF_6); presence of 15.8 M of water in the case of $\mathbf{1}^{+}$. Recording conditions: microwave frequencies, 9.63 GHz (⊥) and 9.41 GHz (//); microwave powers, 1 mW (⊥) and 4 mW (//); modulation amplitude, 1 mT; time constant, 160 ms; T = 5 K. The perpendicular-mode simulated spectrum for **3ox** generated using XSophe is shown in gray. Simulation parameters: $g_x = g_z$ = 1.98; g_y = 2.02; $A_x = A_y = A_z$ = 176 MHz; D = −24 GHz; E/D = 0.16; line widths l_x = 70 mT, $l_y = l_z$ = 10 mT; sigma D = 0.5; sigma E/D = 0.09.

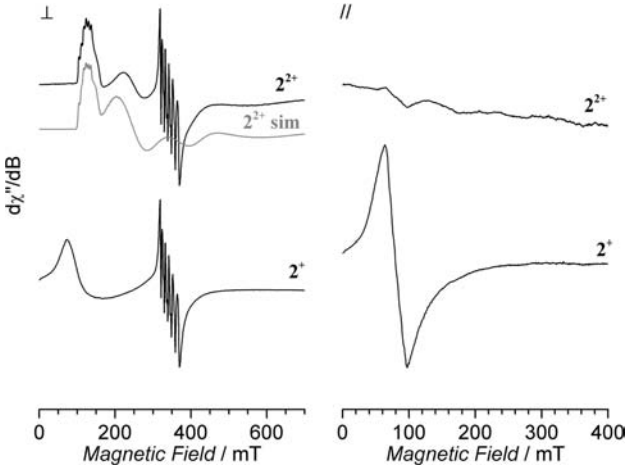

Figure 5. EPR spectra recorded for the chloro complex with perpendicular-mode (left) and parallel-mode (right) detection before (complex $\mathbf{2}^{+}$) and after (complex $\mathbf{2}^{2+}$) exhaustive electrolysis at +1.25 V vs SCE. Experimental conditions: 2 mM solution in CH_3CN (0.1 M Bu_4NPF_6). Recording conditions: microwave frequencies, 9.63 GHz (⊥) and 9.41 GHz (//); microwave powers, 1 mW (⊥) and 4 mW (//); modulation amplitude, 1 mT; time constant, 160 ms; T = 5 K. The perpendicular-mode simulated spectrum for $\mathbf{2}^{2+}$ generated using XSophe is shown in gray. Simulation parameters: g_x = 1.97; g_y = 2.06; g_z = 1.98; A_x = 190 MHz; A_y = 204 MHz; A_z = 174 MHz; D = −24 GHz; E/D = 0.20; line widths $l_x = l_y = l_z$ = 2.2 mT; sigma D = 0.5; sigma E/D = 0.06.

and $\mathbf{3}^{2+}$, the signals are very broad and essentially unresolved with respect to hyperfine structure, although six-line splitting by ~6.9 mT can be distinguished on the feature at 130 mT for $\mathbf{3}^{2+}$ (see Figure S6 in the Supporting Information). The EPR spectra of $\mathbf{1}^{2+}$ and $\mathbf{3}^{2+}$ are virtually identical but differ from that of $\mathbf{2}^{2+}$ which presents narrower and better resolved resonances.

dx.doi.org/10.1021/ic202480h | Inorg. Chem. 2012, 51, 3603−3612

Simulations of the spectra yielded an E/D value of 0.20 in the case of $\mathbf{2}^{2+}$, compared to 0.16 for $\mathbf{1}^{2+}$ and $\mathbf{3}^{2+}$. More significant, a bigger E/D strain and the use of an important line width, particularly along the x-direction, were required to reproduce in the simulations the large features of the spectra of $\mathbf{1}^{2+}$ (gray line in Figure 4) and $\mathbf{3}^{2+}$, compared to $\mathbf{2}^{2+}$ (Figure 5).[39] This reflects a bigger distribution of geometries for the complexes with the oxygenated hydroxy and methoxy ligands, compared to the complex with the chloride ligand. Similar well-resolved EPR and hyperfine features have also been observed previously for manganese complexes in the divalent oxidation state (+II) when a Cl^- anion was present in the coordination sphere.[40,41]

In light of the crystal structure obtained for the Mn(III) complex $\mathbf{1}^+$ showing a pool of water molecules in hydrogen bonding interactions with the HO^- ligand and the fact that such a network can also be envisioned for the lone pairs of the oxygen atom of the methoxo ligand in $\mathbf{3}^+$, it can be proposed that one cause for the strain observed in the Mn(IV) complexes $\mathbf{1}^{2+}$ and $\mathbf{3}^{2+}$ is also the perturbation from the surrounding solvent as the exogenous ligand is conserved during oxidation of the Mn ion.[36] It is likely that the Cl^- anion ligand is less involved in intermolecular interactions with solvent molecules than the other two exogenous ligands, thus leading to less distortion and heterogeneity in the coordination sphere bonds and to a better-resolved spectrum.

UV−Vis Spectroscopy. The electronic absorption spectrum of $\mathbf{1}^+$ (Figure S7(A), dashed line, in the Supporting Information) shows an intense band at 405 nm (Table S7 in the Supporting Information) attributed to a phenolato to Mn(III) charge-transfer transition.[29,42−45] Changes of the absorption spectra upon oxidation at +0.99 V vs SCE were recorded in a spectroelectrochemical cell. During the course of the electrolysis, two intense bands appear at 491 (3680 M^{-1} cm^{-1}) and 668 nm (2520 M^{-1} cm^{-1}). The latter one can be attributed to a phenolate to Mn(IV) LMCT transition.[27,29,46−48] The absence of a transition at ∼1000 nm discards the possible formation of a phenoxyl radical upon oxidation,[38] confirming the Mn(IV) oxidation state attribution for the oxidized complex in agreement with the EPR results. The absorption spectrum of $\mathbf{2}^+$ shows four distinct bands between 310 and 511 nm. Based on comparison with $\mathbf{1}^+$ and other reported chloride Mn(III) complexes, the higher-energy band at 317 nm can be attributed to a Cl^- to Mn(III) charge transfer.[27,40,49,50] The less-intense bands at 480 and 510 nm are similar to those reported in the case of a related chloride Mn(III) complex with no phenolato ligand[40] and can be attributed to Mn(III) d−d transition. A spectroelectrochemical oxidation was also conducted with complex $\mathbf{2}^+$ (see Figure S7B in the Supporting Information). Upon oxidation at 1.25 V vs SCE, three new intense bands appear at 345 nm (10570 M^{-1} cm^{-1}), 598 nm (3248 M^{-1} cm^{-1}), and 786 (3636 M^{-1} cm^{-1}). The two latter bands can be attributed to phenolato to Mn(IV) LMCT bands. The phenolate to Mn(IV) charge transfer band is shifted to higher energy upon replacement of the sixth ligand from chloride (786 nm) to hydroxide (668 nm).[38] Similarly to complex $\mathbf{1}^+$, no evidence of phenoxyl radical formation was detected upon oxidation of $\mathbf{2}^+$. Complex $\mathbf{3}^+$ show results similar to those reported for $\mathbf{1}^+$ (see Table S3 and Figure S7C in the Supporting Information).

We have described the preparation of three mononuclear manganese complexes both in the +III and +IV oxidation states. Cyclic voltammetry (CV) has shown that the +II oxidation state is also accessible for $\mathbf{1}^+$ (upon protonation) and $\mathbf{2}^+$. In the following section, we will investigate the kinetics of the electron transfer for the Mn(IV)/Mn(III) couple in the case of $\mathbf{1}^+$, $\mathbf{2}^+$, and $\mathbf{3}^+$ and for the Mn(III)/Mn(II) couple in the case of $\mathbf{1H}^{2+}$. The peculiar role of the water molecule (in its protonated form for $\mathbf{1H}^{2+}$or deprotonated form for $\mathbf{1}^+$) will be discussed.

Outersphere Electron Transfer Dynamics of $\mathbf{1}^+$, $\mathbf{2}^+$, and $\mathbf{3}^+$, and $\mathbf{1H}^{2+}$. Table 2 shows that, at a given scan rate, the complexes have different peak separation values, indicating different electron transfer kinetics. Therefore, it is interesting to investigate electron-transfer dynamics in order to get new insights into the role of exogenous ligand on the intrinsic parameters controlling electron-transfer dynamics. To accomplish this objective, CV was used to measure, at various temperatures, the electron-transfer standard rate constant (k_S) corresponding to the heterogeneous electron-transfer rate constant at zero driving force. For a given temperature, we obtained the standard rate constant using the procedure of Nicholson.[51] The standard rate constant has the classical form given in eq 1, i.e., the product of a pre-exponential factor, henceforth designated by Z^{het}, whose temperature dependence is negligible, and an exponential term that is dependent on the reorganization energy (λ). In this simplified approach, the effect of a double layer has been omitted. Therefore, it seems more correct to refer to λ as an apparent reorganization energy, including a double-layer effect.[52,53] The parameter λ also contains information regarding internal reorganization of the complex upon electron transfer, as well as solvent reorganization due to charge variation. The pre-exponential factor is related to the electronic coupling between the electrode and the complex and contains information on the electron-transfer adiabaticity, as further detailed later.

$$\ln k_S = \ln(Z^{het}) - \frac{\lambda}{4RT} \tag{1}$$

In order to measure the standard rate constant, cyclic voltammograms have been recorded at several scan rates. Assuming a Butler−Volmer kinetic law for electron transfer with a transfer coefficient $\alpha = 0.5$ (see eq 2), the peak separation is dependent on a single dimensionless parameter Λ ($\Lambda = k_S/(DFv/RT)^{1/2}$, where k_S is the standard rate constant, T the temperature, v the scan rate, F the Faraday constant, R the gas constant, and D the diffusion coefficient).[51,54]

$$\frac{i}{FS} = k_S \exp\left[\frac{F}{2RT}(E - E^0)\right]\left\{[\text{red}] - \exp\left[-\frac{F}{RT}(E - E^0)\right][\text{ox}]\right\} \tag{2}$$

Here, E is the electrode potential, E^0 is the standard potential, the terms that are enclosed by square brackets ($[\cdot]$) are the concentrations at the electrode surface, and S is the electrode surface area. Thus, fitting with a working curve, obtained from simulations using the Digielch program,[55] the variation of peak potentials with scan rate (through a so-called trumpet plot) allows one to evaluate the quantity $k_S/D^{1/2}$. Because the diffusion coefficient D can be determined from the peak current (knowing the electrode surface area), we obtain the standard rate constant from this procedure. Figure 6 shows the voltammograms of $\mathbf{1}^+$ at 293 K at several scan rates, the trumpet plot and simulated voltammograms. Voltammograms at various scan rates and temperatures and the corresponding trumpet plots for $\mathbf{2}^+$, $\mathbf{3}^+$, and $\mathbf{1H}^{2+}$ are shown in the Supporting Information (Figure S8).

dx.doi.org/10.1021/ic202480h | Inorg. Chem. 2012, 51, 3603−3612

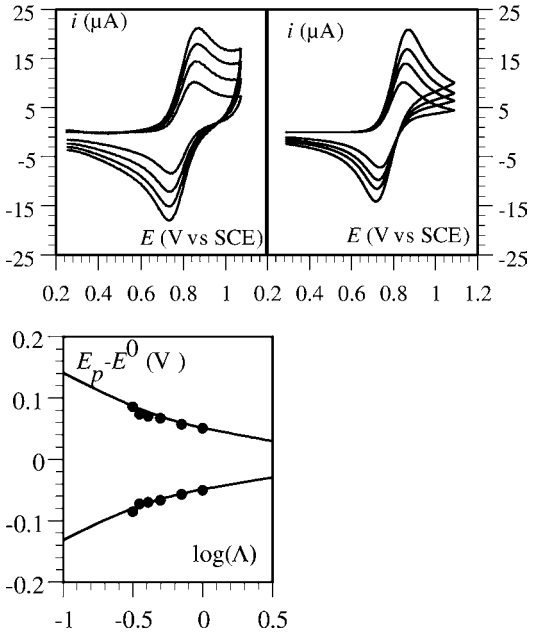

Figure 6. Cyclic voltammetry of $\mathbf{1}^+$ (0.7 mM) at T = 293 K, on a glassy carbon electrode in CH_3CN + 0.1 M NBu_4PF_6 + 15.8 M of H_2O:[36] (upper left) experimental cyclic voltammograms at 0.2, 0.4, 0.6, and 0.8 V/s; (upper right) simulated cyclic voltammograms at 0.2, 0.4, 0.6, and 0.8 V/s, with k_S = 0.0045 cm s^{-1} and $D = 5 \times 10^{-6}$ cm^2 s^{-1}; (lower panel) trumpet plot ($E_p - E^0$ as function of log(Λ); black line represents the theoretical curve fit).

The same procedure has been repeated at various temperatures. A linear Arrhenius plot is obtained upon plotting the experimental standard rate constants against $1/T$, according to eq 1 (see Figure 7a). We thus obtain values of λ = 1.67 eV and Z^{het} = 40 135 cm s^{-1}. Those data may now be compared to those obtained with complexes $\mathbf{2}^+$, $\mathbf{3}^+$, and $\mathbf{1H}^{2+}$ using the very same procedure. Arrhenius plots are given in Figure 7, and data are gathered in Table 3.

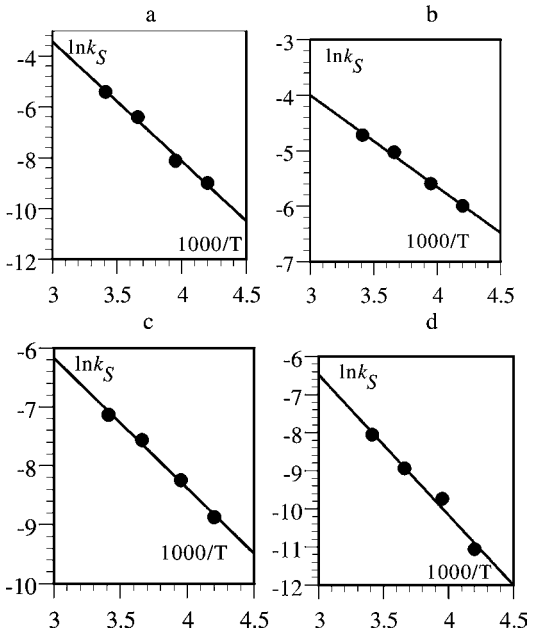

Figure 7. Arrhenius plots using the equation ln $k_S = f(1/T)$: (a) $\mathbf{1}^+$, (b) $\mathbf{2}^+$, (c) $\mathbf{3}^+$, and (d) $\mathbf{1H}^{2+}$. (The line shows the fit according to eq 2.)

Table 3. Pre-exponential Factor and Apparent Reorganization Energy for Complexes $\mathbf{1}^+$ to $\mathbf{1H}^{2+}$

	Z^{het} (cm s^{-1})	λ (eV)	C_0 (eV)
$\mathbf{1}^+$	40125	1.67	1.7×10^{-2}
$\mathbf{2}^+$	2.65	0.57	1.15×10^{-4}
$\mathbf{3}^+$	1.7	0.73	0.74×10^{-4}
$\mathbf{1H}^{2+}$	96	1.27	7.1×10^{-4}

From the reorganization energy values λ, we can distinguish two sets of complexes: $\mathbf{1}^+$ (hydroxo) and $\mathbf{1H}^{2+}$ (aqua) on the one side with large reorganization energies and $\mathbf{2}^+$ (chloride ligand) and $\mathbf{3}^+$ (methoxo ligand) on the other side with low reorganization energies. As shown by Marcus theory, reorganization energy is the sum of two contributions: λ_0, the solvent reorganization energy, and λ_i, the internal reorganization energy due to heavy atoms displacement upon charge transfer. Experiments with $\mathbf{1}^+$ (hydroxo) and $\mathbf{1H}^{2+}$ (aqua) have been performed in a mixture of acetonitrile and water (15.8 M of water), whereas experiments with $\mathbf{2}^+$ (chloride ligand) and $\mathbf{3}^+$ (methoxo ligand) have been performed in pure acetonitrile. At first sight, the differences in reorganization energies could thus be attributed to a larger solvent reorganization energy upon electron transfer in an acetonitrile–water solvent mixture, compared to pure acetonitrile. However, from electrostatic model,[56] solvent reorganization energies are expected to be higher in acetonitrile than in an acetonitrile–water solvent mixture, which is the opposite to the present observation. Moreover, typical solvent reorganization for transition-metal complexes in water are on the order of 0.5–1 eV (i.e., much smaller than the value measured with $\mathbf{1}^+$).[57] As previously discussed, measured standard rate constants are not corrected from the double-layer effect and, therefore, the apparent reorganization energies λ obtained from Arrhenius plots include the double-layer effect. Thus, differences in double-layer effects in both media can contribute to the differences observed on apparent reorganization energies. However, $\mathbf{2}^+$ has lower reorganization energy than $\mathbf{3}^+$, despite a more anodic standard potential, showing that the double-layer effect is not the main factor contributing to the Arrhenius slope. Comparison of $\mathbf{1}^+$ and $\mathbf{1H}^+$ indicates that the maximal double-layer effect contribution upon going from 0.3 V to 0.8 V for the oxidation potential in the acetonitrile–water mixture is 0.4 eV, which is consistent with a small variation of the potential in the outer Helmoltz plane in this range of potential. Therefore, the double-layer effect cannot account for the large differences observed for the apparent reorganization energies. This implies differences in internal reorganization λ_i, i.e., variations of the manganese–exogenous ligand distance and reorganization of the *tBu*L coordination sphere upon charge transfer. Part of the internal reorganization energy is indeed due to the Jahn–Teller effect variation upon oxidation; however, this effect may be considered to be similar for all complexes. Consequently, the variations in reorganization energies observed can be attributed to variations of the manganese–exogenous ligand distances.

The specificity (large reorganization energy) may be related to the ability of the exogenous ligand to form hydrogen bonds (hydroxo and aqua and methoxo to a lesser extent). In that respect, we must emphasize that complex $\mathbf{1}^+$ is studied in the presence of water and that the X-ray structure shows hydrogen

dx.doi.org/10.1021/ic202480h | Inorg. Chem. 2012, 51, 3603–3612

bonds with an interstitial water molecule. This suggests that the second coordination shell around the hydroxo ligand is mainly formed from water molecules and that the reorganization of this shell may be partially responsible for the large internal reorganization energy. Indeed, the present results support the loose solution structure that we previously proposed for $\mathbf{1}^{+}$.[1] The same may be true to a lesser extent with compound $\mathbf{1H}^{2+}$, studied in the presence of a strong acid $HClO_4$ with a large amount of water. On the same line, the ability of the lone pairs of the oxygen of the methoxo ligand to form hydrogen bonds to the residual water present in acetonitrile may also account for the larger reorganization energy of $\mathbf{3}^{+}$ compared to $\mathbf{2}^{+}$. Those conclusions are consistent with the EPR observations discussed earlier.

The second important parameter in electron-transfer dynamics is the pre-exponential factor Z^{het}. From the experimental data, it appears that the hydroxo complex $\mathbf{1}^{+}$ has a very large pre-exponential factor, compared to the other three. Heterogeneous electron transfer is usually assumed to take place at a fixed distance from the electrode (in the Helmholtz Outer Plane), leading to a pre-exponential factor close to the collision factor, $Z^{coll} = [RT/(2\pi M)]^{1/2}$ (M is the molecular mass; thus, $Z^{coll} \simeq 1500$ cm s^{-1} in the present case) if electron transfer is adiabatic (without intervention of solvent dynamics) or significantly lower if electron transfer is nonadiabatic. However, recent works[58,59] have shown that the value of the limiting pre-exponential factor increases when taking into account that the reaction may take place at various distances from the electrode surface. In that context, the large value obtained for $\mathbf{1}^{+}$ is not meaningless and the pre-exponential factor may be described by the expression

$$Z^{het} = \frac{\nu_n}{\beta}\frac{\pi}{\sqrt{1+\frac{\pi RT}{\lambda}}}\ln\left(1+\frac{2\pi^2 {C_0}^2}{h\nu_n\sqrt{4\pi RT\lambda}}\right) \quad (3)$$

where ν_n is the effective nuclear vibration frequency (typically 10^{12} s^{-1}), C_0 the electronic coupling constant between the electrode and the substrate at the minimal approach distance, and β the decay constant for the coupling constant with the electrode−substrate distance (typically 1 Å^{-1}). From eq 3, since the value of Z^{het} is not very sensitive to the value of λ, a working curve representing $\log(Z^{het})$, as a function of $\log(C_0)$, can be drawn for typical values of ν_n, β, and λ (Figure 8). From this working curve, we obtain the values of the electronic coupling constant for all four complexes (see Table 3).

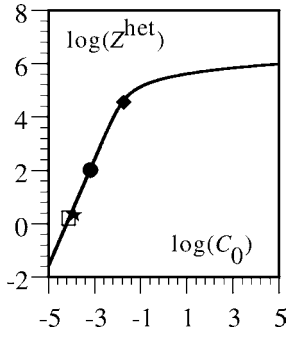

Figure 8. Working curve (solid line, according to eq 3) representing log Z^{het}, as a function of log C_0. Experimental data: (◆) $\mathbf{1}^{+}$, (□) $\mathbf{2}^{+}$, (★) $\mathbf{3}^{+}$, and (●) $\mathbf{1H}^{+}$.

It appears that the hydroxo complex $\mathbf{1}^{+}$ has an electronic coupling constant that is 2 orders of magnitude larger than that of the other complexes. In other words, this complex has an electronic wave function with a better ability to overlap with the empty electrode electronic states. We may interpret this feature as an indication that the electronic density is more delocalized over the exogenous ligand in the case of hydroxo than in the case of other ligands (aqua > methoxo > chlorido). The water molecules in the second coordination sphere serve as a bridge to facilitate electron transfer from the complex to the electrode and allow to achieve longer-range electron transfer. To support the proposed view of the hydroxo complex being wired to the electrode via water molecules, one must recall that (i) water forms clusters in acetonitrile[60,61] and (ii) glassy carbon surfaces contain hydroxyl or oxo functionalities that have an affinity for water.

CONCLUSION

As was discussed previously, the formation of the mononuclear $[t\mathrm{Bu}\mathrm{LMn(III)OH}]^{+}$ complex $\mathbf{1}^{+}$ by air oxidation of the transient manganese(II) complex is in sharp contrast with the formation of the dinuclear mono-μ-oxo $[\mathrm{LMn^{3+}(O)Mn^{3+}L}]^{2+}$ complex observed for the unsubstituted ligand L^{-}.[1] The mononuclear structure of $\mathbf{1}^{+}$ is conserved in the +IV oxidation state, indicating low acidity of the hydroxide ligand in $\mathbf{1}^{2+}$. This last point indicates a strong donating effect of the *tert*-butyl groups not only on the distance of the Mn−O bond, but also on the reactivity of the coordinated hydroxide ligand.

The role of the hydroxide ligand on the kinetics of the electron transfer for the Mn(IV)/Mn(III) couple is addressed based on comparison with two identical complexes having a chloride ($\mathbf{2}^{+}$) or methoxide ($\mathbf{3}^{+}$) ion as the exogenous ligand. In the case of the Mn(III)/Mn(II) couple, the role of the aqua ligand ($\mathbf{1H}^{2+}$) is investigated. It is shown that $\mathbf{1}^{+}$ presents a larger reorganization energy (λ) than $\mathbf{2}^{+}$ and $\mathbf{3}^{+}$. We propose that this specificity is related to the ability of the exogenous OH^{-} ligand to form hydrogen bonds with water molecules from the second coordination sphere, with the reorganization of this shell being partially responsible for the large internal reorganization energy. The same trend is observed in the case of the $\mathbf{1H}^{2+}$ complex for the Mn(II)/Mn(III) couple, for which the H_2O exogenous ligand offers possible hydrogen bonding.

The measurement of the electron transfer constant k_S also gives access to the electronic coupling constant C_0 between the electrode and the substrate. The larger coupling constant that is measured in the case of $\mathbf{1}^{+}$ is attributed to the hydrogen-bonded OH^{-} ligand that facilitate delocalization of the electronic density over the ligand, then allowing more-efficient electron transfer. The effect of hydrogen-bonded ligands on the modulation of fragmental charge transfer from ligand to a metal center already has been experimentally investigated in the case of Ni bacteriochlorophyll.[62] The authors demonstrated the modulation of the ligand electronic structure and the metal charge density due to ligand−solvent hydrogen-bond interactions. In the present case, we show experimentally that ligand−solvent hydrogen-bond interactions influence the dynamics of electron transfer in Mn complexes. These findings are of particular interest within the framework of the studies devoted to the comprehension of the OEC catalytic site, and in a more general interest, since hydrogen bonding has been shown to directly affect the properties and reactivity of the redox-center in both biological and nonbiological catalysis.

dx.doi.org/10.1021/ic202480h | Inorg. Chem. 2012, 51, 3603−3612

■ ASSOCIATED CONTENT

Supporting Information

Crystallographic data for $2(PF_6)$ and $3(ClO_4)$ and selected angles for $1(ClO_4)$, $2(PF_6)$, and $3(ClO_4)$. ORTEP view of 1^+, 2^+, and 3^+. Cyclic voltammetry for 1^+, 2^+, and 3^+. UV−Vis absorption spectra recorded during the course of the electrochemical oxidation of 1^+, 2^+, and 3^+. Enlarged view of the parallel-mode EPR spectrum of 1^+, 2^+, and 3^+, as well as an enlarged view of the perpendicular-mode EPR spectrum of 1^{2+} and 3^{2+}. UV−Vis absorption spectrum of $1H^{2+}$. Cyclic voltammetry evolution of 1^+ upon addition of proton. Cyclic voltammetry at various temperatures and scan rates and trumpet plots for 1^+, 2^+, 3^+, and $1H^{2+}$. Effect of ohmic drop compensation on peak potential for a ferrocene solution.This material is available free of charge via the Internet at http://pubs.acs.org.

■ AUTHOR INFORMATION

Corresponding Author

*E-mail: elodie.anxolabehere@univ-paris-diderot.fr.

Notes

The authors declare no competing financial interest.

■ ACKNOWLEDGMENTS

This work was financially supported by ANR-PROTOCOLE (ANR-07-BLAN-0280) and ANR-TAKE CARE (ANR- 2010-BLAN-0808), European Project SOLAR-H2, FP7 Contract 212508 Institut de Chimie Moléculaire et des Matériaux d'Orsay.

■ REFERENCES

(1) El Ghachtouli, S.; Lassalle-Kaiser, B.; Dorlet, P.; Guillot, R.; Anxolabéhère-Mallart, E.; Costentin, C.; Aukauloo, A. *Energy Environ. Sci.* **2011**, *4*, 2041.

(2) Yano, J.; Yachandra, V. K. *Inorg. Chem.* **2008**, *47*, 1711−1726.

(3) Zouni, A.; Witt, H.-T.; Kern, J.; Fromme, P.; Krauß, N.; Saenger, W.; Orth, P. *Nature* **2001**, *409*, 739−743.

(4) Ferreira, K. N.; Iverson, T. M.; Maghlaoui, K.; Barber, J.; Iwata, S. *Science* **2004**, *303*, 1831−1838.

(5) Yano, J.; Kern, J.; Sauer, K.; Latimer, M. J.; Pushkar, Y.; Biesiadka, J.; Loll, B.; Saenger, W.; Messinger, J.; Zouni, A.; Yachandra, V. K. *Science* **2006**, *314*, 821−825.

(6) Guskov, A.; Kern, J.; Gabdulkhakov, A.; Broser, M.; Zouni, A.; Saenger, W. *Nat. Struct. Mol. Biol.* **2009**, *16*, 334−342.

(7) Umena, Y.; Kawakami, K.; Shen, J.-R.; Kamiya, N. *Nature* **2011**, *473*, 55−60.

(8) Babcock, G. T.; Tommos, C. *Acc. Chem. Res.* **1998**, *31*, 18−25.

(9) Messinger, J. *Phys. Chem. Chem. Phys.* **2004**, *6*, 4764−4771.

(10) McEvoy, J. P.; Brudvig, G. W. *Chem. Rev.* **2006**, *106*, 4455−4483.

(11) Pecoraro, V. L.; Hsieh, W.-Y. *Inorg. Chem.* **2008**, *47*, 1765−1778.

(12) Meelich, K.; Zaleski, C. M.; Pecoraro, V. L. *Philos. Trans. R. Soc. London, Ser. B* **2008**, *363*, 1271−1281.

(13) Dau, H.; Limberg, C.; Reier, T.; Risch, M.; Roggan, S.; Strasser, P. *ChemCatChem* **2010**, *2*, 724−761.

(14) Sproviero, E. M.; Gascón, J. A.; McEvoy, J. P.; Brudvig, G. W.; Batista, V. S. *Coord. Chem. Rev.* **2008**, *252*, 395−415.

(15) Mullins, C. S.; Pecoraro, V. L. *Coord. Chem. Rev.* **2008**, *252*, 416−443.

(16) Borovik, A. S. *Acc. Chem. Res.* **2005**, *38*, 54−61.

(17) Goldsmith, C. R.; Cole, A. P.; Stack, D. T. *J. Am. Chem. Soc.* **2005**, *127*, 9904−9912.

(18) Eroy-Reveles, A. A.; Leung, Y.; Beavers, C. M.; Olmstead, M. M.; Mascharak, P. K. *J. Am. Chem. Soc.* **2008**, *130*, 4447−4458.

(19) Sawant, S. C.; Wu, X.; Cho, J.; Cho, K.-B.; Kim, S. H.; Seo, M. S.; Lee, Y.-M.; Kubo, M.; Ogura, T.; Shaik, S.; Nam, W. *Angew. Chem., Int. Ed.* **2010**, *49*, 8190−8194.

(20) Horner, O.; Anxolabéhère-Mallart, E.; Charlot, M.-F.; Tchertanov, L.; Guilhem, J.; Mattioli, T. A.; Boussac, A.; Girerd, J.-J. *Inorg. Chem.* **1999**, *38*, 1222−1232.

(21) Larrow, J. F.; Jacobsen, E. N.; Gao, Y.; Hong, Y.; Nie, X.; Zepp, C. M. *J. Org. Chem.* **1994**, *59*, 1939−1942.

(22) Stoll, S.; Schweiger, A. *J. Magn. Reson.* **2006**, *178*, 42−55.

(23) Hanson, G. R.; Gates, K. E.; Noble, C. J.; Griffin, M.; Mitchell, A.; Benson, S. *J. Inorg. Biochem.* **2004**, *98*, 903−916.

(24) Lexa, D.; Savéant, J.-M.; Zickler, J. *J. Am. Chem. Soc.* **1977**, *99*, 2786−2797.

(25) Sheldrick, G. M.; *SHELXS-97*; University of Göttingen: Göttingen, Germany, 1997.

(26) Farrugia, L. J. *J. Appl. Crystallogr.* **1997**, *30*, 565.

(27) Sabater, L.; Hureau, C.; Blain, G.; Guillot, R.; Thuéry, P.; Rivière, E.; Aukauloo, A. *Eur. J. Inorg. Chem.* **2006**, 4324−4337.

(28) Sabater, L.; Hureau, C.; Guillot, R.; Aukauloo, A. *Inorg. Chem.* **2006**, *45*, 2373−2375.

(29) Neves, A.; Erthal, S. M. D.; Vencato, I.; Ceccato, A. S.; Mascarenhas, Y. P.; Nascimento, O. R.; Hörner, M.; Batista, A. A. *Inorg. Chem.* **1992**, *31*, 4749−4755.

(30) Sabater, L.; Guillot, R.; Aukauloo, A. *Tetrahedron Lett.* **2005**, *46*, 2923−2926.

(31) Reddig, N.; Pursche, D.; Rompel, A. *J. Chem. Soc., Dalton Trans.* **2004**, 1474−1480.

(32) Shirin, Z.; Young, V. G. Jr.; Borovik, A. S. *Chem. Commun.* **1997**, 1967−1968.

(33) Hubin, T. J.; McCormick, J. M.; Alcock, N. W.; Busch, D. H. *Inorg. Chem.* **2001**, *40*, 435−444.

(34) Lassalle-Kaiser, B.; Hureau, C.; Pantazis, D. A.; Pushkar, Y.; Guillot, R.; Yachandra, V. K.; Yano, J.; Neese, F.; Anxolabéhère-Mallart, E. *Energy Environ. Sci.* **2010**, *3*, 924−938.

(35) Experiments with 2^+ and 3^+ cannot be performed in the presence of 15.8 M of water, in comparison to 1^+ in the same medium, because of the exogeneous ligand displacement.

(36) In the case of 1^+, the quasi-reversibility is obtained when the acetonitrile solution is not water-free. When recorded in extremely dry acetonitrile, the Mn(III)/Mn(IV) oxidation process is irreversible. The origin of this behavior has been detailed in the previous paper.[1]

(37) Groni, S.; Blain, G.; Guillot, R.; Policar, C.; Anxolabéhère-Mallart, E. *Inorg. Chem.* **2007**, *46*, 1951−1953.

(38) Kurahashi, T.; Kikuchi, A.; Tosha, T.; Shiro, Y.; Kitagawa, T.; Fujii, H. *Inorg. Chem.* **2008**, *47*, 1674−1686.

(39) Simulation of EPR spectra of 3^{2+} are identical to those reported for complex 1^{2+}.

(40) Groni, S.; Hureau, C.; Guillot, R.; Blondin, G.; Blain, G.; Anxolabéhère-Mallart, E. *Inorg. Chem.* **2008**, *47*, 11783−11797.

(41) Hureau, C.; Blondin, G.; Charlot, M.-F.; Philouze, C.; Nierlich, M.; Césario, M.; Anxolabéhère-Mallart, E. *Inorg. Chem.* **2005**, *44*, 3669−3683.

(42) Cisnetti, F.; Lefèvre, A.-S.; Guillot, R.; Lambert, F.; Blain, G.; Anxolabéhère-Mallart, E.; Policar, C. *Eur. J. Inorg. Chem.* **2007**, 472−4480.

(43) Patch, M. G.; Carrano, C. J. *Inorg. Chim. Acta* **1981**, *56*, L71.

(44) Bonadies, J. A.; Maroney, M. J.; Pecoraro, V. L. *Inorg. Chem.* **1989**, *28*, 2044−2051.

(45) Diril, H.; Chang, H.-R.; Nigles, M. J.; Zhang, X.; Potenza, J. A.; Schugar, H. J.; Isied, S. S.; Hendrickson, D. N. *J. Am. Chem. Soc.* **1989**, *111*, 5102−5114.

(46) Hureau, C.; Blondin, G.; Charlot, M.-F.; Philouze, C.; Nierlich, M.; Césario, M.; Anxolabéhère-Mallart, E. *Inorg. Chem.* **2005**, *44*, 3669−3683.

(47) Hureau, C.; Sabater, L.; Gonnet, F.; Blain, G.; Sainton, J.; Anxolabéhère-Mallart, E. *Inorg. Chim. Acta* **2006**, *359*, 339−345.

(48) Baldwin, M. J.; Stemmler, T. L.; Riggs-Gelasco, P. J.; Kirk, M. L.; Penner-Hahn, J. E.; Pecoraro, V. L. *J. Am. Chem. Soc.* **1994**, *116*, 11349−11356.

(49) Sarneski, J. E.; Thorp, H. H.; Brudvig, G. W.; Crabtree, R. H.; Schulte, G. K. *J. Am. Chem. Soc.* **1990**, *112*, 7255−7260.
(50) Goodwin, H. A.; Sylva, R. N. *Aust. J. Chem.* **1965**, *18*, 1743−1749.
(51) Nicholson, R. S. *Anal. Chem.* **1965**, *37*, 1351−1355.
(52) The standard rate constant $k_{S,corr}$ is related to the apparent standard rate constant (k_S) measured experimentally, according to: $k_{S,corr} = k_S \exp[(2z + 1)F\phi_2/(2RT)]$, where z is the charge number of the reactant and ϕ_2 is the potential in the outer Helmoltz plane (i.e., the potential at the boundary between the compact double layer and the diffuse double layer).[53]
(53) Delahay, P. *Double Layer and Electrode Kinetics*; Interscience Publishers: New York, 1965.
(54) Savéant, J.-M. In *Elements of Molecular and Biomolecular Electrochemistry*; Wiley−Interscience: New York, 2006; Chapter 1, pp 50−53.
(55) Rudolph, M. *J. Electroanal. Chem.* **2003**, *543*, 23−39.
(56) Marcus, R. A. In *Special Topics in Electrochemistry*; Rock, P. A., Ed.; Elsevier: New York, 1977; pp 161−179.
(57) Sutin, N.; Brunschwig, B. S. *ACS Symp. Series* **1982**, *198*, 105.
(58) Feldberg, S. W.; Sutin, N. *Chem. Phys.* **2006**, *324*, 216.
(59) Costentin, C.; Robert, M.; Savéant, J.-M. *Phys. Chem. Chem. Phys.* **2010**, *12*, 13061−13069.
(60) Marcus, Y. *J. Chem. Soc. Faraday Trans. 1* **1989**, *85*, 381−388.
(61) Marcus, Y. *J. Chem. Soc. Faraday Trans. 1* **1990**, *86*, 277−281.
(62) Yerushalmi, R.; Brandis, A.; Rosenbach-Belkin, V.; Baldridge, K. K.; Scherz, A. *J. Phys. Chem.* **2006**, *110*, 412.